XLVI CILAMCE
VITÓRIA - ES - BRAZIL - 2025
XLVI IBERO-LATIN AMERICAN CONGRESS ON COMPUTATIONAL METHODS IN ENGENEERING

Assessment of the effects of the temporal state in the numerical simulation of the airflow around a storage pile in the presence of a cubic bulding

Matheus de Araujo Siqueira[1], Bruno Furieri[1], Jean-Luc Harion[2,3]

[1]*Programa de Pós Graduação em Engenharia Ambiental, Universidade Federal do Espírito Santo*
Av. Fernando Ferrari, 514, 29075-910, Vitória/ES, Brasil
matheus.siqueira@edu.ufes.br, bruno.furieri@ufes.br
[2]*Centre for Materials and Processe, IMT Nord Europe, Institut Mines-Télécom*
Bd Lahure, 764, 59500, Douai, France
[3]*LGCgE, Laboratory of Civil Engineering and Geo-Environment, ULR 4515, University of Lille, IMT Nord Europe, University of Artois*
F-59000, Lille, France
jean-luc.harion@imt-nord-europe.fr

Abstract. Diffuse emissions of granular material from storage piles open to the atmosphere represent an important source of pollution by industrial sites. Thus, to better deal with its impacts, a good understanding of the airflow around piles at small scales is vital, for example, at the characteristic scale of an industrial site. In this sense, Computational Fluid Dynamics (CFD) numerical simulations are largely applied. However, recent works have reported non-symmetric results for the airflow around the storage pile. This is not expected for this kind of geometrical case. The present work evaluates the influence, in terms of symmetry, of numerically simulating the airflow around the storage pile in a steady and unsteady state, using the open source software OpenFOAM-v2312. It was shown that the cubic building presence induces several instabilities in the airflow. Such instabilities cause convergence problems in the steady state solution and produce non-symmetric results. On the other hand, through an unsteady simulation, it was possible to capture the instabilities well and thus obtain averaged symmetric results. Second-order upwind methods were used.

Keywords: Granular Storage Pile, Computational Fluid Dynamics, Temporal Discretization, Symmetry

1 Introduction

Storage piles of granular materials open to the atmosphere represent a substantial source of fugitive emissions due to wind erosion in large industrial sites [1]. Such emissions reduce air quality and also can cause risk to human health [2–9]. Thus, a good understanding of the airflow around storage piles is vital to better deal with this environmental issue. In this sense, to perform a local-scale characterization of the airflow and understand its details, Computational Fluid Dynamics (CFD) simulations pose an essential tool.

Furthermore, the CFD simulations are frequently used to perform an estimation of the particle emission in such sources [1, 10–20]. Which, in general, depends on local meteorology, material properties, and the shape/size of the pile, being based on the wall shear stress along the pile. The most widely used model for conducting such estimation was posed by the United States Environmental Protection Agency (USEPA). This method is based on the subdivision of the pile surface into regions of a constant ratio between the surface wind speed and the approaching wind speed (u_s/u_r), followed by the calculation of an erosion potential for each of these subareas. The total emission of the pile is calculated as the sum of the contribution of each subarea for an N number of perturbations [21].

To study the airflow and the particle emission around a storage pile in the presence of a cubic building, Ferreira et al. [22] combined wind tunnel experiments and CFD simulations. However, the author reported non-symmetric results for the numerical simulations of the airflow, which is not expected for this kind of geometry. This suggests that this airflow could present an unsteady, even bistable nature that is not well captured through the steady-state solution performed by the author. That is, the presence of the cubic building $45°$ angled can cause an instability in the airflow, resulting in vortex-shedding behavior in the airflow downstream of the cubic building and storage pile. With this in mind, the present work assesses, using the open-source software OpenFOAM v2312, the

effect of conducting the numerical simulation of the storage pile in the presence of a cubic building in a steady and unsteady state in terms of symmetry.

2 Methodology

The present study focuses on a geometry first presented by Ferreira et al. [22] and shown in Figure 1 along with its dimensions and boundary conditions. This consists of a storage pile in the presence of a cubic obstacle $45°$ angled in the longitudinal direction.

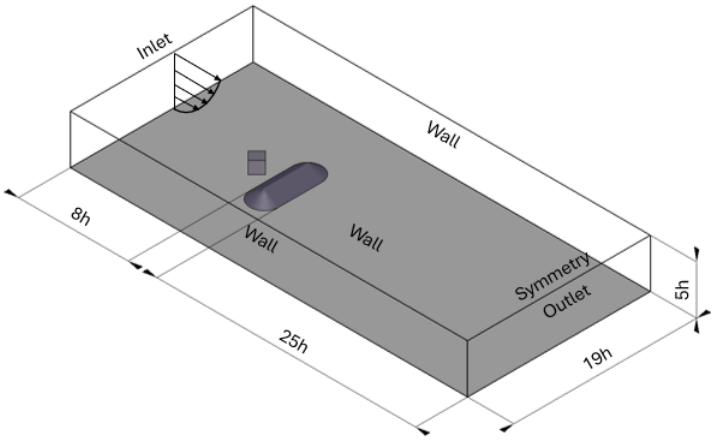


Figure 1. Computational domains and boundary conditions based on the height of the storage pile height ($h = 77\ mm$).

The height of the storage pile is equal to $h = 77\ mm$ (h), width equal to $236\ mm$, length equal to $579\ mm$ and rest angle equal to $34.5°$. The cubic building edge (H_b) is equal to $100\ mm$ and the gap between the storage pile and the cubic building is equal to $0.5 * H_b$. The Reynolds number of the fluid flow is approximately equal to 68000, based on the freestream velocity and the height of the cubic building.

The $3D$ airflow field is modeled using the Navier-Stokes equations. Where the continuity equation is shown in 1a and the momentum conservation in 1b. To deal with the turbulent fluctuating effects, a U-RANS approach was used, specifically an unsteady solution of the $k-\omega\ SST$ turbulence model [23]. Where the turbulent kinectic energy balance equation is shown in 1c and the specific dissipation balance equation shown in 1d.

$$\frac{\partial \overline{u}}{\partial x_i} = 0 \tag{1a}$$

$$\rho\frac{\partial \overline{u}_i}{\partial t} + \rho\overline{u}_j\frac{\partial \overline{u}_i}{\partial x_j} = -\frac{\partial \overline{P}}{\partial x_i} + \frac{\partial}{\partial x_j}\left[\mu\left(\frac{\partial \overline{u}_i}{\partial x_j} + \frac{\partial \overline{u}_j}{\partial x_i}\right) - \rho\overline{u_i' u_j'}\right] \tag{1b}$$

$$\frac{\partial \rho\kappa}{\partial t} + u_j\frac{\partial \rho\kappa}{\partial x_j} = \tau_{i,j}\frac{\partial u_i}{\partial x_j} - \beta^*\rho\omega\kappa + \frac{\partial}{\partial x_j}\left[(\mu + \sigma_\kappa\mu_T)\frac{\partial \kappa}{\partial x_j}\right] \tag{1c}$$

$$\frac{\partial \rho\omega}{\partial t} + u_j\frac{\partial \rho\omega}{\partial x_j} = \frac{\gamma}{\upsilon_t}\tau_{i,j}\frac{\partial u_i}{\partial x_j} - \beta\rho\omega^2 + \frac{\partial}{\partial x_j}\left[(\mu + \sigma_w\mu_T)\frac{\partial \omega}{\partial x_j}\right] + 2(1-F_1)\rho\sigma_\omega 2\frac{1}{\omega}\frac{\partial k}{\partial x_j}\frac{\partial \omega}{\partial x_j} \tag{1d}$$

where u is the velocity component ($m\ s^{-1}$) and i, j are the indexes, being $(i, j) = (1, 2, 3)$ and, consequently, $(u_1, u_2, u_3) = (u, v, w)$ and $(x_1, x_2, x_3) = (x, y, z)$, ρ is the specific mass ($kg\ m^{-3}$), P is the thermodynamic pressure ($kg\ m^{-1}\ t^{-2}$) and μ the dynamic viscosity of the fluid ($kg\ m^{-1}\ t^{-1}$), $\beta*$, σ_κ, γ, β, σ_ω are the constants of the model, υ_t is the turbulent eddy viscosity ($m^2\ s^{-2}$) and F_1 is an auxiliary function.

Concerning the boundary conditions, for the inlet fully developed turbulent profiles of velocity (U_{mag}), turbulent kinetic energy (k), and specific dissipation rate (ω) are set, all obtained via a periodic precursor domain. At the outlet, a zero normal gradient condition (outflow condition) is set, in which it is assumed that all flow variables, except the pressure, are fully developed. At the walls, for the sides and bottom faces of the domain, the cubic building, and the storage pile, a non-slip condition ($u_1 = u_2 = u_3 = 0$) is set. For the upper boundary, a condition of symmetry is set, in which all the gradients of the normal variables are set to zero. The boundary conditions

were set based on the numerical calculations performed by Ferreira et al. [22] and Furieri et al. [24]. All boundary conditions are summarized in Table 1.

	Boundary conditions		
Location	Momentum	κ	ω
Inlet	Developed profiles		
Outlet	$\partial\phi/\partial n = 0$		
Top	$\partial\overline{u}/\partial y = 0; \partial\overline{v}/\partial z = 0; \overline{w} = 0$	$\partial\kappa/\partial y = 0$	$\partial\omega/\partial y = 0$
Left and right walls	$u_1 = u_2 = u_3 = 0$	$\kappa = 0$	$\omega = 0$
Bottom, building and pile surface	$u_1 = u_2 = u_3 = 0$	$\kappa = 0$	$\omega = 0$

Table 1. Boundary conditions to be used in the present work numerical simulations.

In Figure 2, a lateral view of the computational mesh is shown. To ensure y^+ ($y^+ = \rho u^* d/\mu$) below 5 for the first element close to the regions in which no-slip condition boundary condition were set, the height of the first element were equal to $1.2E-04\ m$. The outer region of the domain, close to the top, is meshed with level 1. In the lower region, level 2 is defined. For the transition close to the walls, a level 3 mesh is set, and for the storage pile and the cubic building, the transition is meshed with level 5.

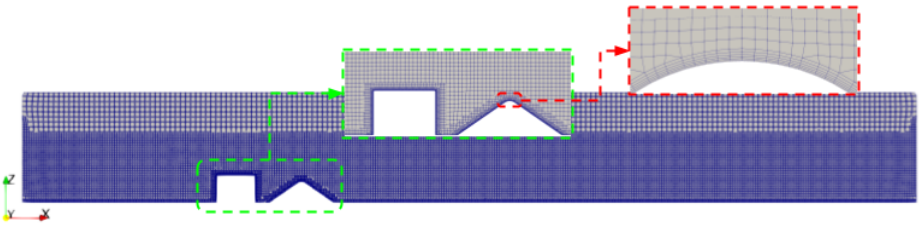


Figure 2. Lateral view of the discretized domain plotted in the central plane in the main airflow direction with a zoom on the storage pile top for the three constructed meshes.

For the pressure-momentum coupling, the PIMPLE algorithm was used. For the unsteady simulations, an Euler first-order scheme was used for temporal discretization. In this method, the time step is automatically adjusted by always setting the Courant number below one throughout the simulation. The size of the time step was, in general, on the order of $5 \cdot 10^{-5}\ s$. The simulation time was set to 0.5 seconds for stabilization and 4.5 seconds for the average calculation. All residuals were set to 10^{-4}. All simulations were performed using the open-source OpenFOAM v2312 software.

Spetial atention were given to the order of the spatial discretization of the momentum, turbulent kinetic energy, and specific dissipation equations. It is known that while first-order upwind discretization yelds better convergence, it is also associated with numerical diffusion errors and thus less accurate results when compared to the second-order upwind discretization. On the other hand, despite its higher accuracy the second-order upwind method are prone to instabilities and convergence issues. An example of a first and second order upwind discretization applied to a advective term ($u\left(\frac{\partial\phi}{\partial x}\right)$) is shown in Equation 2a and 2b, respective. Where ϕ is the quantity being advected. The present work uses the second-order upwind scheme for both steady and unsteady solutions.

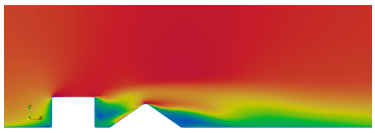
$$u\left(\frac{\partial\phi}{\partial x}\right) \equiv \begin{cases} u\left(\frac{\phi_i - \phi_{i-1}}{\delta x}\right), & \text{if } u > 0 \\ u\left(\frac{\phi_{i+1} - \phi_i}{\delta x}\right), & \text{if } u < 0 \end{cases} \tag{2a}$$

$$u\left(\frac{\partial\phi}{\partial x}\right) \equiv \begin{cases} u\left(\frac{3\phi_i - 4\phi_{i-1} + \phi_{i-2}}{\delta x}\right), & \text{if } u > 0 \\ u\left(\frac{-3\phi_i + 4\phi_{i-1} - \phi_{i-2}}{\delta x}\right), & \text{if } u > 0 \end{cases} \tag{2b}$$

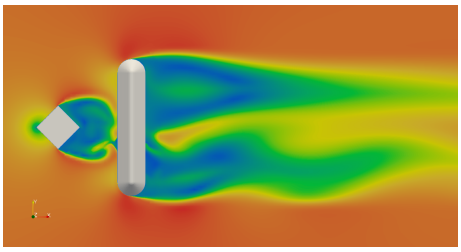
3 Results

Through Figure 3, when comparing the solution given by both simulation states, it is seen that several instabilities occur in the airflow that aren‘t well captured by the steady solution. This feature seems to cause two concerns. A first is that despite the fact that the instabilities aren’t well captured, they are still influencing the numerical results and probably causing the convergence problems discussed in the next paragraph. A second is that, even though it is intended to have an average result and not the instantaneous values and their instabilities, it seems to be essential to take into account the contribution of the temporal instabilities to calculate a symmetric averaged airflow. Thus it is seen that only the simulations conducted in an unsteady state produced symmetrical results.

Steady Solution

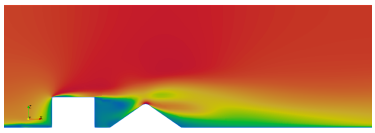


(a) Lateral view - Steady solution

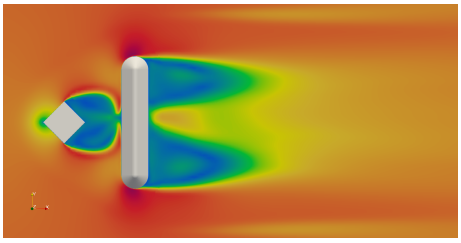


(b) Top view view - Steady solution

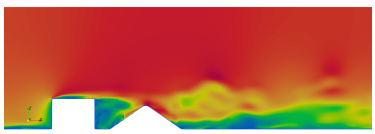
Unsteady Solution



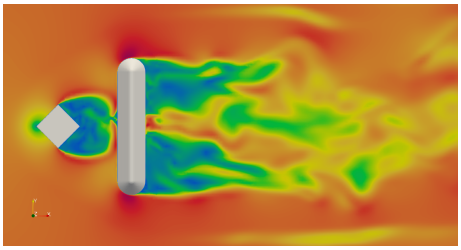
(c) Lateral view - averaged



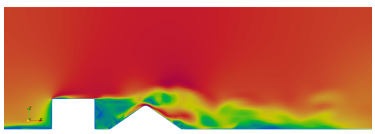
(d) Top view view - averaged



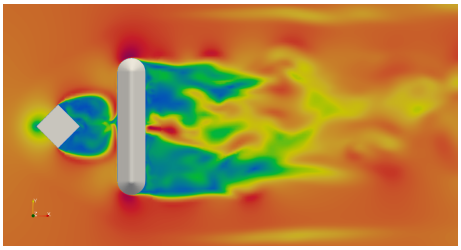
(e) Lateral view - $t = 4.00s$



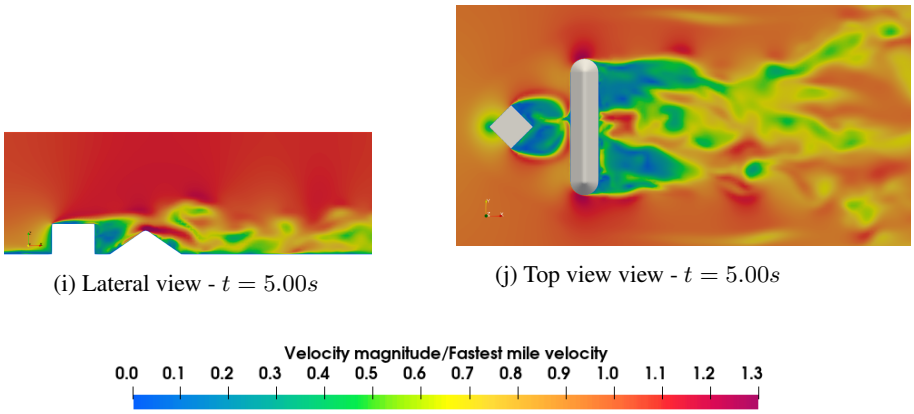
(f) Top view view - $t = 4.00s$



(g) Lateral view - $t = 4.50s$



(h) Top view view - $t = 4.50s$

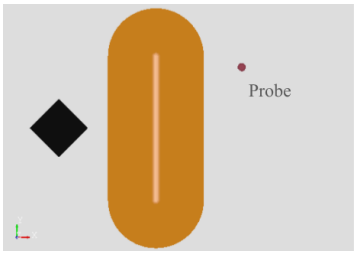


(i) Lateral view - $t = 5.00s$

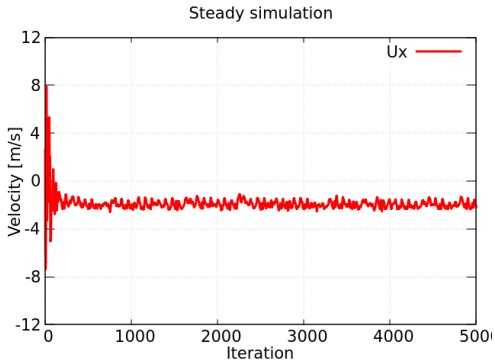
(j) Top view view - $t = 5.00s$

Figure 3. Velocity contours plotted at the central plane (lateral view) and at a plane distant $0.5 * H_b$ from the bottom (top view).

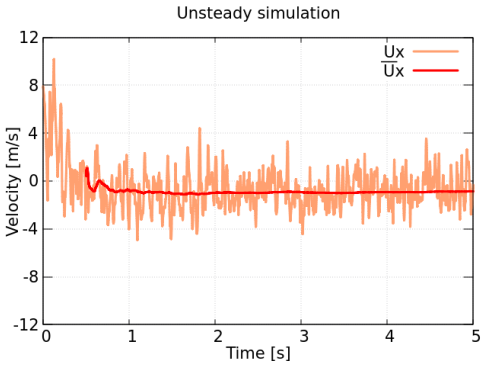
As mentioned earlier, the first-order upwind method can suppress some important airflow instabilities and thus provide good stability; however, it can lead to inaccurate results. On the other hand, the second-order upwind method better captures the airflow instabilities and thus can lead to convergence problems. That behavior can be seen in Figure 4, where it is shown that velocity monitors for both simulation states. The noisy pattern presented by the steady simulation seems to evidence the convergence problems when dealing with the instabilities captured by the method. Otherwise, for the unsteady simulations, that problem seems to be attenuated by its temporal solution, and it is possible to obtain a constant average solution. For the unsteady simulation, the Courant number was kept below one throughout the simulation, which also made a great contribution to the simulation stability.



(a) Location of the monitors



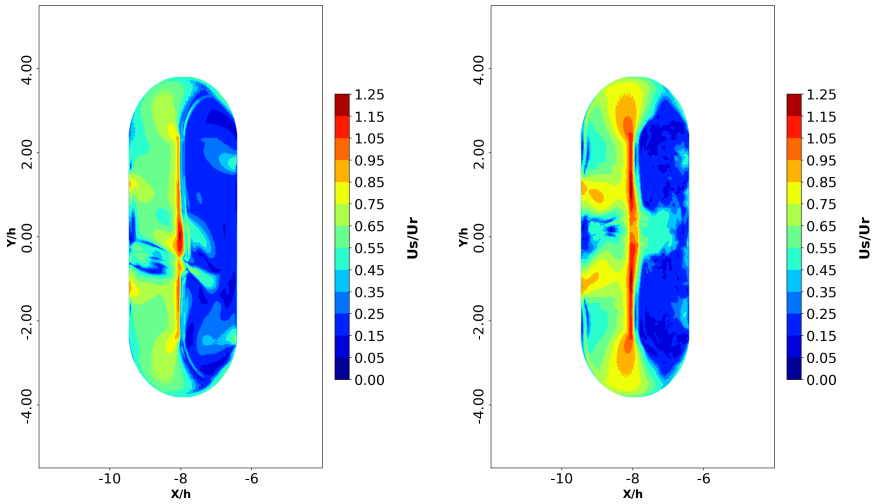
(b) Velocity monitor: Steady state simulation



(c) Velocity monitor: Unsteady state simulation

Figure 4. Velocity monitor (Location: $(-5.20h, -1.95h, 0.65h)$).

It is important to note that a poor solution of the airflow will also possess a great impact on the subsequent steps of characterizing the storage pile emissions. As mentioned in section 1, the US-EPA emission model is based on the subdivision of the storage pile surface in regions with constant u_s/u_r. As shown in Figure 5, the u_s/u_r distribution for both simulation are quite different in shape and values. When applyng the US-EPA model for both simulations, a emission rate of $1.82\ gs^{-1}$ is found for the steady simulations and $2.61\ gs^{-1}$, a 30% difference.



(a) Steady solution (b) Unsteady solution

Figure 5. Distribution of u_s/u_r velocity ratio over the storage pile

4 Conclusions

The present work analyzed the influence of the temporal state on the numerical simulation of the airflow in a geometrical case containing a storage pile and a cubic building. Through the simulations, it was shown that due to the unsteady characteristics of the airflow, steady state simulations lead to non-symmetrical results and convergence problems. The unsteady simulations using second-order upwind methods make it possible to capture the airflow temporal instabilities and lead to symmetrical averaged results. It was also shown a 30% difference in the granular particle emission rate calculated through the US-EPA model when using as inlet data the steady and unsteady numerical simulation results.

Acknowledgements. The authors acknowledge the sponsorship from Co-ordenação de Aperfeiçoamento de Pessoal de Nıvel Superior (CAPES), Conselho Nacional de Desenvolvimento Cientıfico e Tecnológico (CNPq) and Fundação de Amparo à Pesquisa do Espırito Santo (FAPES).

Authorship statement. The authors hereby confirm that they are the sole liable persons responsible for the authorship of this work, and that all material that has been herein included as part of the present paper is either the property (and authorship) of the authors, or has the permission of the owners to be included here.

References

[1] O. Bouarour, A. McNabola, B. Grosso, B. Considine, A. Lai, F. Pinna, and V. Dentoni. 3d numerical simulation of airflow structure and dust emissions from an open storage pile behind a dynamic solid fence-deflector. *Atmospheric Environment: X*, vol. 21, pp. 100245, 2024.

[2] M. R. Miller. Oxidative stress and the cardiovascular effects of air pollution. *Free Radical Biology and Medicine*, vol. 151, pp. 69–87, 2020.

[3] J. Sigaux, J. Biton, E. André, L. Semerano, and M.-C. Boissier. Air pollution as a determinant of rheumatoid arthritis. *Joint Bone Spine*, vol. 86, n. 1, pp. 37–42, 2019.

[4] H. Bové, E. Bongaerts, E. Slenders, E. M. Bijnens, N. D. Saenen, W. Gyselaers, P. Van Eyken, M. Plusquin, M. B. J. Roeffaers, M. Ameloot, and T. S. Nawrot. Ambient black carbon particles reach the fetal side of human placenta. *Nature Communications*, vol. 10, n. 1, 2019.

[5] A. Seaton, L. Tran, R. Chen, R. L. Maynard, and L. J. Whalley. Pollution, particles, and dementia: A hypothetical causative pathway. *International Journal of Environmental Research and Public Health*, vol. 17, n. 3, pp. 862, 2020.

[6] X. Li, M. Zhang, Y. Jiang, X. Zhao, L. Wang, J. Zhu, X. Xu, Z. Li, J. Jia, and D. Zhu. Air curtain dust-collecting technology: An experimental study on the performance of a large-scale dust-collecting system. *Journal of Wind Engineering and Industrial Aerodynamics*, vol. 220, pp. 104875, 2022.

[7] R. Naidu, B. Biswas, I. R. Willett, J. Cribb, B. Kumar Singh, C. Paul Nathanail, F. Coulon, K. T. Semple, K. C. Jones, A. Barclay, and R. J. Aitken. Chemical pollution: A growing peril and potential catastrophic risk to humanity. *Environment International*, vol. 156, pp. 106616, 2021.
[8] T. Faherty, J. E. Raymond, G. McFiggans, and F. D. Pope. Acute particulate matter exposure diminishes executive cognitive functioning after four hours regardless of inhalation pathway. *Nature Communications*, vol. 16, n. 1, 2025.
[9] V. J. Williams, R. Trane, K. Sicinski, P. Herd, M. Engelman, and S. Asthana. Midlife and late-life environmental exposures on dementia risk in the wisconsin longitudinal study: The modifying effects of apoe. *Alzheimer's & Dementia*, vol. 20, n. 12, pp. 8263–8278, 2024.
[10] X. Cong, S. Cao, Z. Chen, S. Peng, and S. Yang. Impact of the installation scenario of porous fences on wind-blown particle emission in open coal yards. *Atmospheric Environment*, vol. 45, n. 30, pp. 5247–5253, 2011.
[11] C. Turpin and J. L. Harion. Effects of flattening the stockpile crest and of the presence of buildings on dust emissions from industrial open storage systems. In *Air Pollution XVII*, volume 1 of *AIR09*, pp. 419–430. WIT Press, 2009a.
[12] C. Turpin and J.-L. Harion. Numerical modeling of flow structures over various flat-topped stockpiles height: Implications on dust emissions. *Atmospheric Environment*, vol. 43, n. 35, pp. 5579–5587, 2009b.
[13] C. Turpin and J.-L. Harion. Effect of the topography of an industrial site on dust emissions from open storage yards. *Environmental Fluid Mechanics*, vol. 10, n. 6, pp. 677–690, 2010.
[14] C.-P. Yeh, C.-H. Tsai, and R.-J. Yang. An investigation into the sheltering performance of porous windbreaks under various wind directions. *Journal of Wind Engineering and Industrial Aerodynamics*, vol. 98, n. 10–11, pp. 520–532, 2010.
[15] X. Cong, S. Yang, S. Cao, Z. Chen, M. Dai, and S. Peng. Effect of aggregate stockpile configuration and layout on dust emissions in an open yard. *Applied Mathematical Modelling*, vol. 36, n. 11, pp. 5482–5491, 2012.
[16] T. Badr and J. Harion. Quantification of diffuse dust emissions from open air sources on industrial sites. In *3rd IASME/WSEAS International Conference on Energy, Environment and Sustainable Development EEESD*, volume 7, pp. 276–280, 2007.
[17] J. Toraño, R. Rodriguez, I. Diego, J. Rivas, and A. Pelegry. Influence of the pile shape on wind erosion cfd emission simulation. *Applied Mathematical Modelling*, vol. 31, n. 11, pp. 2487–2502, 2007.
[18] T. Badr and J. Harion. Numerical modelling of flow over stockpiles: Implications on dust emissions. *Atmospheric Environment*, vol. 39, n. 30, pp. 5576–5584, 2005.
[19] M. G. Badas, V. Dentoni, F. Angius, and F. Pinna. Numerical investigation on the pm emission potential of metal sulphides open storage. *Atmosphere*, vol. 13, n. 9, pp. 1417, 2022.
[20] L. Novak, B. Bizjan, J. Pražnikar, B. Horvat, A. Orbanić, and B. Širok. Numerical modeling of dust lifting from a complex-geometry industrial stockpile. *Strojniški vestnik - Journal of Mechanical Engineering*, vol. 61, n. 11, pp. 621–631, 2015.
[21] USEPA. 13.2.5 industrial wind erosion. *Compilation of Air Pollution Emission Factors*, vol. 1, 2006.
[22] M. C. S. Ferreira, B. Furieri, de C. L. Morais, J. F. Stocco, N. C. Reis, J.-L. Harion, and J. M. Santos. Experimental and numerical investigation of building effects on wind erosion of a granular material stockpile. *Environmental Science and Pollution Research*, vol. 27, n. 29, pp. 36013–36026, 2020.
[23] F. R. Menter. Two-equation eddy-viscosity turbulence models for engineering applications. *AIAA Journal*, vol. 32, pp. 1598–1605, 1994.
[24] B. Furieri, de C. L. Morais, J. M. Santos, and J.-L. Harion. Wind tunnel and cfd analysis of dust re-emission potential from ground regions around successive stockpiles. *Journal of the Brazilian Society of Mechanical Sciences and Engineering*, vol. 45, n. 12, 2023.